Fluorescence detection of Mn²⁺, Cr₂O₇²⁻ and nitroexplosives and photocatalytic degradation of methyl violet and rhodamine B based on two stable metal–organic frameworks†

Yu Wu,[*a] Jian Wu,[b] Zhidong Luo,[c] Jun Wang,[a] Yulong Li,[a] Yaoyao Han[c] and Jianqiang Liu[*c]

The reaction of $Zn(NO_3)_2 \cdot 6H_2O/Cd(NO_3)_2 \cdot 4H_2O$ with a semi-flexible ligand 4′-(4-(3,5-dicarboxylphenoxy)phenyl)-4,2′:6′,4″-terpyridine (H_2dbp) gave two new metal–organic frameworks of [Zn(dbp)]$_n$ (**1**) and [Cd(dbp)(H$_2$O)·2H$_2$O·CH$_3$CN]$_n$ (**2**). Single crystal X-ray diffraction analyses reveal that both **1** and **2** show three-dimensional, two-fold interpenetrating four-connected networks with $4^4.6^{10}.8$ topology. The photoluminescence investigation indicates that both **1** and **2** could be prospective candidates for developing luminescence sensors for the sensing of Mn²⁺, Cr₂O₇²⁻ and nitroaromatic analytes. Furthermore, the photocatalysis properties of **1**–**2** for the degradation of methyl violet and rhodamine B were examined.

Metal–organic frameworks (MOFs) are a fascinating class of materials that have been extensively studied because of their rich structural chemistry and potential applications in numerous areas, including gas storage and separation, catalysis, and chemical sensing.[1–5] The organic ligands containing an aromatic π-conjugated system are subject to excitation, giving rise to photoluminescence (PL) upon irradiation. In addition, the metal components can also contribute to the PL, in which case d¹⁰-metal are often involved. Naturally, these luminescent MOFs (LMOFs) are used for the efficient, economic, and portable fluorometers, greatly promoting research and development in this subject area.[6–11] Recently, considerable research effort has been focused on the potential applications of MOFs in photocatalysis.[12,13] However, the building of MOFs with specific properties still remains a challenge because there are so many factors influencing the resulting polymers.[14,15]

It has been proposed that aromatic organic ligands play an important role in interacting with the substrate.[16,17] On the basis of the previously mentioned points, a pyridine carboxylate ligand of 4′-(4-(3,5-dicarboxylphenoxy)phenyl)-4,2′:6′,4″-terpyridine (H_2dbp), which contains both carboxylate and pyridine donor moieties, was selected, which can help enrich the coordination modes. As far as is known, the MOFs based on H_2dbp have been not explored extensively to date.[18] Recently, a series of MOFs with a dbp ligand have been designed and synthesized and their degradation of methyl violet (MV) has been examined.[18a] Continuing the interest in the structures and properties of M-dbp architectures, in this paper, the assembly of H_2dbp with zinc/cadmium (Zn²⁺/Cd²⁺) centers in two 3D microporous MOFs, [Zn(dbp)]$_n$ (**1**) and [Cd(dbp)(H$_2$O)·2H$_2$O·CH$_3$CN]$_n$ (**2**), are reported, which represent a new category of two-fold interpenetrating four-connected networks in the dbp system. The luminescence sensors and photocatalysis properties for the degradation of MV and rhodamine B (RhB) of **1**–**2** were evaluated and discussed.

Materials and method

All the other reagents used for the syntheses were commercially available and employed without further purification. Powder X-ray diffraction (PXRD) was performed on a Bruker D8 ADVANCE X-ray diffractometer with Cu-Kα radiation ($\lambda = 1.5418$ Å) at 50 kV, 20 mA with a scanning rate of 6° per min and a step size of 0.02°. Fourier transform infrared (FT-IR) spectra were collected using a potassium bromide pellet were measured using a Nicolet Impact 750 FTIR spectrometer in the range of 400–4000 cm⁻¹. Thermogravimetric analysis (TGA) was performed under a nitrogen (N₂) atmosphere from room temperature to 900 °C at a heating rate of 10 °C min⁻¹. The

[a]*Institute of Functional Materials, Sichuan University of Science & Engineering, Zigong, 643000, PR China. E-mail: wuyuhlj@163.com; Fax: +86-813-5505605; Tel: +86-813-5505605*

[b]*Guangxi Key Laboratory of Chemistry and Engineering of Forest Products, Guangxi University for Nationalities, College of Chemistry and Chemical Engineering, Nanning, Guangxi 530006, China*

[c]*School of Pharmacy, Guangdong Medical University, Dongguan, 523808, China. E-mail: jianqiangliu2010@126.com*

photocatalytic activity studies were carried out using a Shimadzu UV-Vis 2501PC spectrophotometer.

The PL sensing was performed as follows: the PL properties of **1–2** were investigated in *N,N*-dimethylformamide (DMF) emulsions at room temperature using a Shimadzu RF-5301PC spectrofluorophotometer. The **1–2**–DMF emulsions were prepared by adding 3 mg of **1–2** powder into 3.00 mL of DMF and then ultrasonically agitating the mixture for 30 min before testing.

The photocatalytic reactions were performed as follows: 50 mg of **1–2** were dispersed in a 50 mL aqueous solution of MV or RhB (10 mg L^{-1}) under stirring in the dark for 30 min to ensure the establishment of an adsorption–desorption equilibrium. Then the mixed solution was exposed to ultraviolet (UV) irradiation from a mercury (Hg) lamp (250 W) and kept under continuous stirring during irradiation for 100 min. Samples (5 mL) of the mixture were removed every 10 min and collected by centrifugation for analysis using UV-Visible (Vis) spectrometer. By contrast, a simple control experiment was also performed under the same conditions without adding any catalysts.

X-ray crystallography

Single crystal X-ray diffraction data were collected on a Bruker SMART APEX X-ray diffractometer that was equipped with graphite monochromated MoKα radiation ($\lambda = 0.71073$ Å) by using an ω-scan technique. The intensities were corrected for absorption effects by using the Siemens Area Detector ABSorption correction program (SADABS). The structure was solved using SHELXL-97.[19] All the hydrogen atoms were generated geometrically and refined isotropically using a riding model. All non-hydrogen atoms were refined using anisotropic displacement parameters. Crystallographic details and selected bond dimensions for **1–2** are listed in Tables S1 and S2 (ESI†), respectively. CCDC numbers are: 1515961 and 1502038.

Syntheses

[Zn(dbp)]$_n$ (1). A mixture of zinc nitrate hexahydrate (Zn(NO$_3$)$_2$·6H$_2$O; 0.0297 g, 0.1 mmol), 4′-(4-(3,5-dicarboxylphenoxy)phenyl)-4,2′:6′,4″-terpyridine (H$_2$dbp; 0.0489 g, 0.1 mmol) and sodium hydroxide (NaOH; 0.0400 g, 0.1 mmol) in acetonitrile (CH$_3$CN; 3 mL) and deionised water (3 mL) was stirred for 30 min in air. Then the resulting solution was transferred into in a Teflon-lined stainless steel vessel (25 mL), which was then sealed and heated to 140 °C for 72 h. The solution was cooled to room temperature at a rate of 5 °C h^{-1}, and yellow block crystals of **1** were obtained (yield = 39% based on Zn). Anal. calcd (%) for C$_{29}$H$_{17}$ZnN$_3$O$_5$, C, 63.01; H, 3.10; N, 7.60. Found C, 62.68; H, 3.16; N, 7.71.

[Cd(dbp)(H$_2$O)·2H$_2$O·CH$_3$CN]$_n$ (2). A mixture of cadmium nitrate tetrahydrate (Cd(NO$_3$)$_2$·4H$_2$O; 0.0308 g, 0.1 mmol), and H$_2$dbp (0.0489 g, 0.1 mmol) in CH$_3$CN (3 mL) and deionised water (3 mL) was stirred for 30 min in air. Then the resulting solution was transferred into a Teflon-lined stainless steel vessel (25 mL), which was then sealed and heated to 160 °C for 72 h, and yellow needle-like crystals of **2** were obtained

(yield = 52% based on Cd). Anal. calcd (%) for C$_{62}$H$_{52}$Cd$_2$N$_8$O$_{16}$, C, 53.57; H, 3.77; N, 8.06. Found C, 53.34; H, 3.52; N, 9.09.

The two materials were characterized using infrared spectroscopy (IR) and TGA, and the results are shown in Fig. S1 (ESI) and S2 (ESI†). The PXRD patterns indicated that **1–2** remains crystalline upon desolvation (Fig. S3; ESI†). PXRD patterns (Fig. S4a; ESI†) confirmed that the crystallinity of **1** when it was soaked at different pHs of the medium, although it was likely that there were structural and/or symmetry changes, especially at low pHs. However, under different pHs, no major changes to the PXRD patterns of **2** were detected, which confirmed its stability (Fig. S4b; ESI†). To assess the porosity of **1** and **2**, the N$_2$ sorption isotherm was performed at 77 K, which displayed a type-I isotherm with the Brunauer–Emmett–Teller surface areas of 201.3 and 10.9 m^2 g^{-1}, respectively, and the full details are shown in Fig. S5 (ESI†).

Results and discussion

Crystal structures

[Zn(dbp)]$_n$ (1). The asymmetric unit contains one Zn(II) atom and one dbp ligand. The Zn(II) is coordinated by two oxygen atoms and two nitrogen atoms from two adjacent dbp ligand linkers to give the ZnO$_2$N$_2$ tetrahedral geometry (Fig. 1a). The Zn–O/N bond lengths are in the range of 1.951(4)–2.030(5) Å, which are comparable to those reported in other related Zn(II) polymers.[20] The completely deprotonated dbp ligand shows a bi(monodentate) coordinated manner (see Scheme S1; ESI†). The Zn(II) cations are bridged by dbp linkers which give rise to a complicated 3D network (Fig. 1b and c). The large voids directed by a single 3D net allow incorporation of one identical motif, providing a two-fold interpenetrating network (Fig. 1d). Better insight into the elegant framework of **1** can be accessed using a topology method. In this analysis, the metal center can be viewed as a 4-connected node. In this way, this net can be
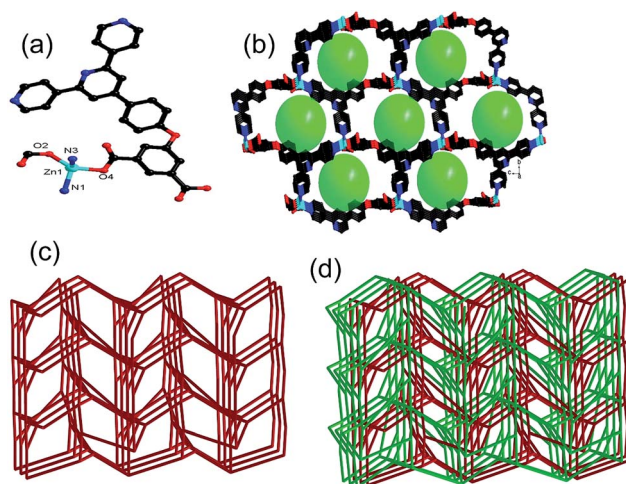

Fig. 1 (a) Coordination environments of Zn(II) atoms in **1**; (b) ball-and-stick representation of the 3D porous structure in **1**; (c) view of 4-connected networks with 4^4.6^{10}.8 topology; (d) view of two-fold interpenetrating net. All the hydrogen atoms are omitted for clarity.

simplified as $4^4.6^{10}.8$ topology (Fig. 1c). The total solvent volume in the lattices is about 3067.9 Å^3 (30.7% of the unit cell) as calculated using the PLATON suite of programs.[21]

$[Cd(dbp)(H_2O)\cdot 2H_2O\cdot CH_3CN]_n$ **(2).** To investigate the influence of metal cations in constructing coordination frameworks, **2** was obtained by the reaction of dbp with $Cd(NO_3)_2\cdot 4H_2O$. Compound **2** is isostructural to **1** but with a different coordination environment of the metal site and a slightly bigger unit cell (Fig. 2a–c). Because of the large radius of Cd(II), both carboxylate groups in the dbp ligand in **2** show bisdentate coordination to the Cd(II) ions (Scheme S1†). Each Cd(II) atom adopts a distorted CdO_5N_2 geometry coordinated by four oxygen atoms and two nitrogen atoms from two adjacent dbp and one coordinated water molecule (Fig. 2a). The Cd(II) centers are also linked together by dbp to produce a 3D two-fold interpenetrating architecture with 4-connected $4^4.6^{10}.8$ topology (Fig. 2c). Upon removal of the CH_3CN and H_2O molecules, **2** forms a microporous framework containing 16.7% solvent accessible voids.[21]

Luminescence sensing

Because of the existence of available voids in **1–2,** their fluorescence responses to small molecules, cations and anions were measured. The PL spectra of **1** and **2** were recorded (Fig. S6; ESI†). It has been reported that the free H_2dbp ligand shows emission at 550 nm (λ_{ex} = 404 nm).[18b] Compared to the free H_2dbp ligand, **1–2** show an emission at 393 and 405 nm (λ_{ex} = 315 nm), respectively. The features of the luminescent properties of **1–2** are mostly attributed to the emission of the organic linker.[22] In order to explore the luminescent responses of **1–2** to metal ions, **1–2** was dispersed in DMF solutions containing different $M(NO_3)_x$ salts (M = Ag$^+$, Ca^{2+}, Cd^{2+}, Co^{2+}, Hg$^+$, K$^+$, Li$^+$, Mg^{2+}, Mn^{2+}, Na$^+$, Ni^{2+}, Pb^{2+}, Zn^{2+}) as microcrystalline solids for
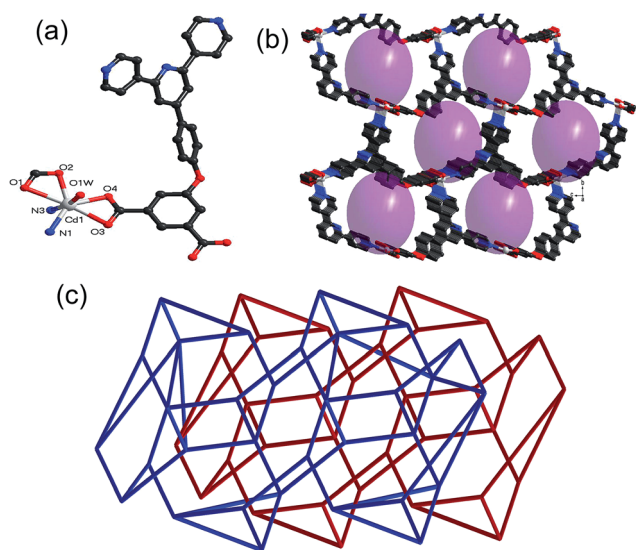

Fig. 2 (a) Coordination environments of Cd(II) atoms in **2**; (b) ball-and-stick representation of the 3D porous structure in **2**; (c) view of two-fold interpenetrating net. All the hydrogen atoms are omitted for clarity.

potential luminescent sensing studies. Interestingly, the luminescent intensity of the samples was dependent on the nature of the metal ions. The luminescent properties of M^{n+}@1/2 are recorded and listed in Fig. 3a and 4a. The intensity of **1–2** is slightly enhanced by the addition of Ca^{2+}, Li$^+$, and Mg^{2+} (Fig. S7 and S8; ESI†), however, Mn^{2+} almost quenches the luminescence of **1–2,** indicating that there is highly selective sensing of Mn^{2+} ions by **1–2** through this quenching effect.[23] The PXRD patterns of **1–2** indicated their basic frameworks are kept upon dispersion in the metal ion solutions (Fig. S3; ESI†). To quantitatively investigate the response behavior of **1–2** towards Mn^{2+} ions, the emission spectra of **1–2** in the presence of different concentrations of Mn^{2+} ions in DMF were measured at room temperature. The luminescent intensity of **1–2** is almost completely quenched at an $Mn(NO_3)_2$ concentration of 37.5 × 10^{-4} and 60 × 10^{-5} M, respectively. Furthermore, a linear correlation for $(I_0 - I)/I_0$ and the concentration of Mn^{2+} ions was obtained, and following the 3δ/slope, the detection limits of 1.80 × 10^{-4} M and 5.08 × 10^{-6} M were calculated for **1** and **2,** respectively, (Fig. S8†),[18c] which is higher relative to reported examples. The luminescent measurements indicate that the different anions have a great influence on the luminescent intensity of **1** and **2**. The $Cr_2O_7^{2-}$ ion has the largest quenching effect on the emission of **1–2** (Fig. 3c and 4c). The luminescent intensity of **1–2** decreased to 50% at concentrations of 15 × 10^{-4} and 10 × 10^{-5} M (Fig. 3d and 4d), respectively. It has been reported that the Mn^{2+} and $Cr_2O_7^{2-}$ ions may compete for the absorption of light with the organic molecules and thus reduce the efficiency of energy transfer from ligand to ions.[24,25]

The remarkable fluorescence and stability of **1–2** led to the investigation of its potential for fluorescence sensing of nitroexplosives (Fig. 3e and 4e).[26–28] Thus, the DMF suspension of **1–2** was chosen for use in the detection of different kinds of nitroexplosives, including 2,4-dinitrotoluene (2,4-DNT), 2,6-dinitrotoluene (2,6-DNT), 2,4,6-trinitrotoluene (TNT), 2-nitrotoluene (2-NT), 4-nitrotoluene (4-NT) and 1,3-dinitrobenzene (1,3-DNB). These six nitro compounds can weaken the PL intensity of **1–2** to different degrees. The order of quenching efficiency is TNT > 4-NT > 2,4-DNT > 2-NT ≈ 1,3-DNB > 2,6-DNT. This efficiency is comparable to that of other MOFs in sensing TNT.[9,26] Compared with 2,6-DNT and 1,3-DNB, TNT shows the strongest quenching effect, which may be ascribed to the fact that it has the strongest π-stacking between polymer and analyte. This phenomenon was observed in Zn/Cd–MOFs.[26c] Therefore, **1** and **2** can be used to distinguish between nitroaromatic molecules with different numbers of –NO$_2$ groups. As shown in Fig. 3f and 4f, with the increase of TNT concentration, the luminescence intensity of **1–2**@TNT suspension decreases distinctly. The maximum fluorescent intensity of **1–2** was reduced by 95% upon exposure to 19 × 10^{-5} and 10 × 10^{-5} M solutions of TNT. The fluorescence quenching efficiency can be quantitatively explained by the Stern–Volmer (SV) equation: $(I_0/I) = 1 + K_{sv}[Q]$,[29,30] where K_{sv} is the quenching constant (M^{-1}), and [Q] is the molar concentration of the analyte (M). The SV plots for TNT in **1–2** are linear at low concentrations, with a K_{sv} value of 4.35 × 10^4 and 1.38 × 10^5 M^{-1}, respectively, and are among the higher values for MOF-based TNT sensors (Fig. S7 and
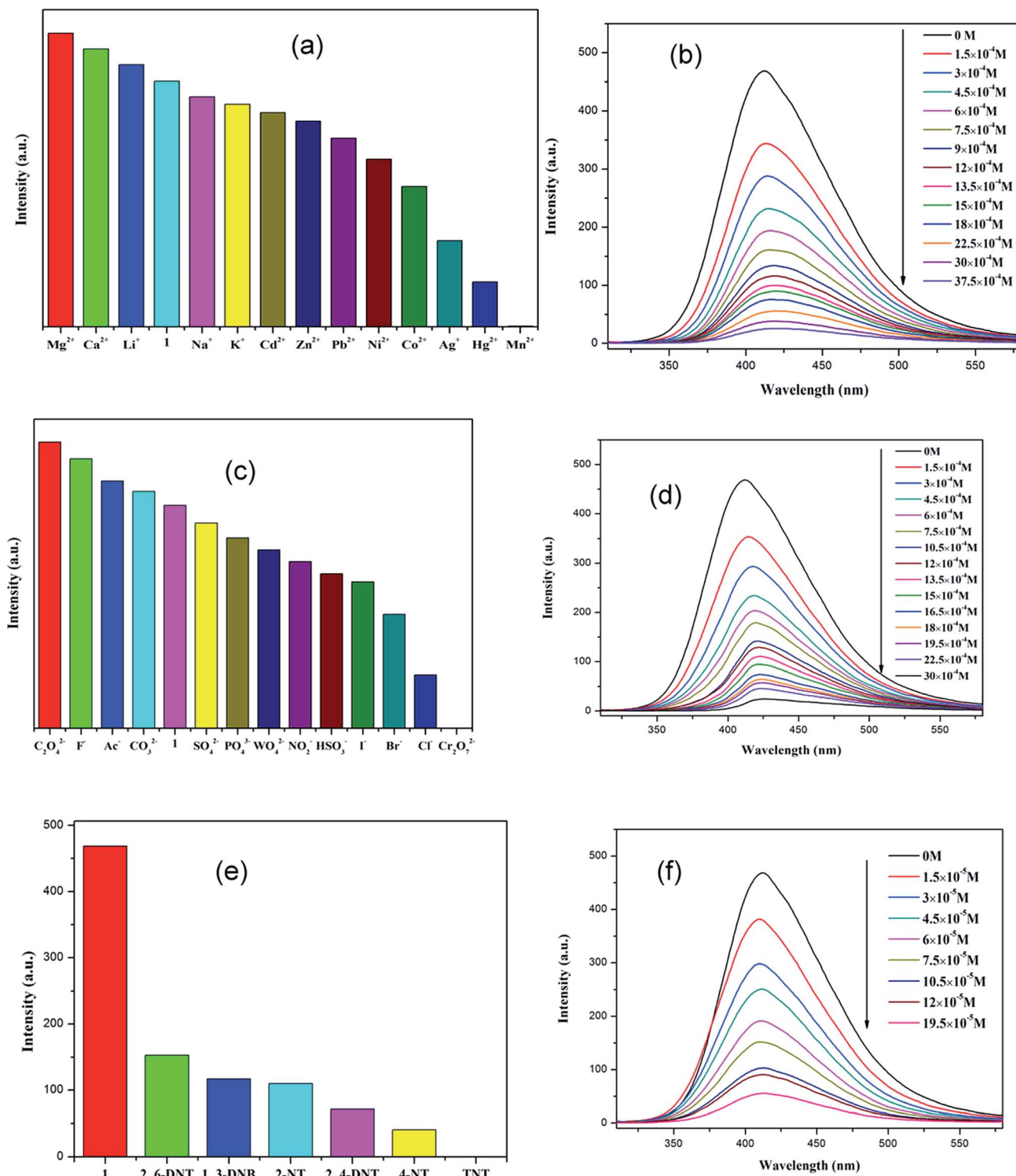
Fig. 3 (a), (c) and (e) Emission spectra of **1** in different metal ions, anions and nitro-explosives (excited at 315 nm). (b), (d) and (f) Emission spectra of **1** in different concentrations of metal ions, anions and nitro-explosives in DMF (excited at 315 nm).

S8; ESI†).[28] The high quenching constant for TNT reveals that **1–2** are excellent sensors for sensitive and selective detection of TNT. As shown in Fig. 3e and 4e, the rates of quenching of the Zn(II) polymer **1** was faster with the analyte than that of Cd(II) polymer **2**. Thus, the observed quenching trend is not controlled by a single factor, such as the nature of the analyte molecules, metal centers and relative orbital energies and interactions between coordination polymers and analyte molecules.

In the anion, cation and nitro-explosives used in this research, Mn^{2+}, $Cr_2O_7^{2-}$ and a series of nitro-explosives were all
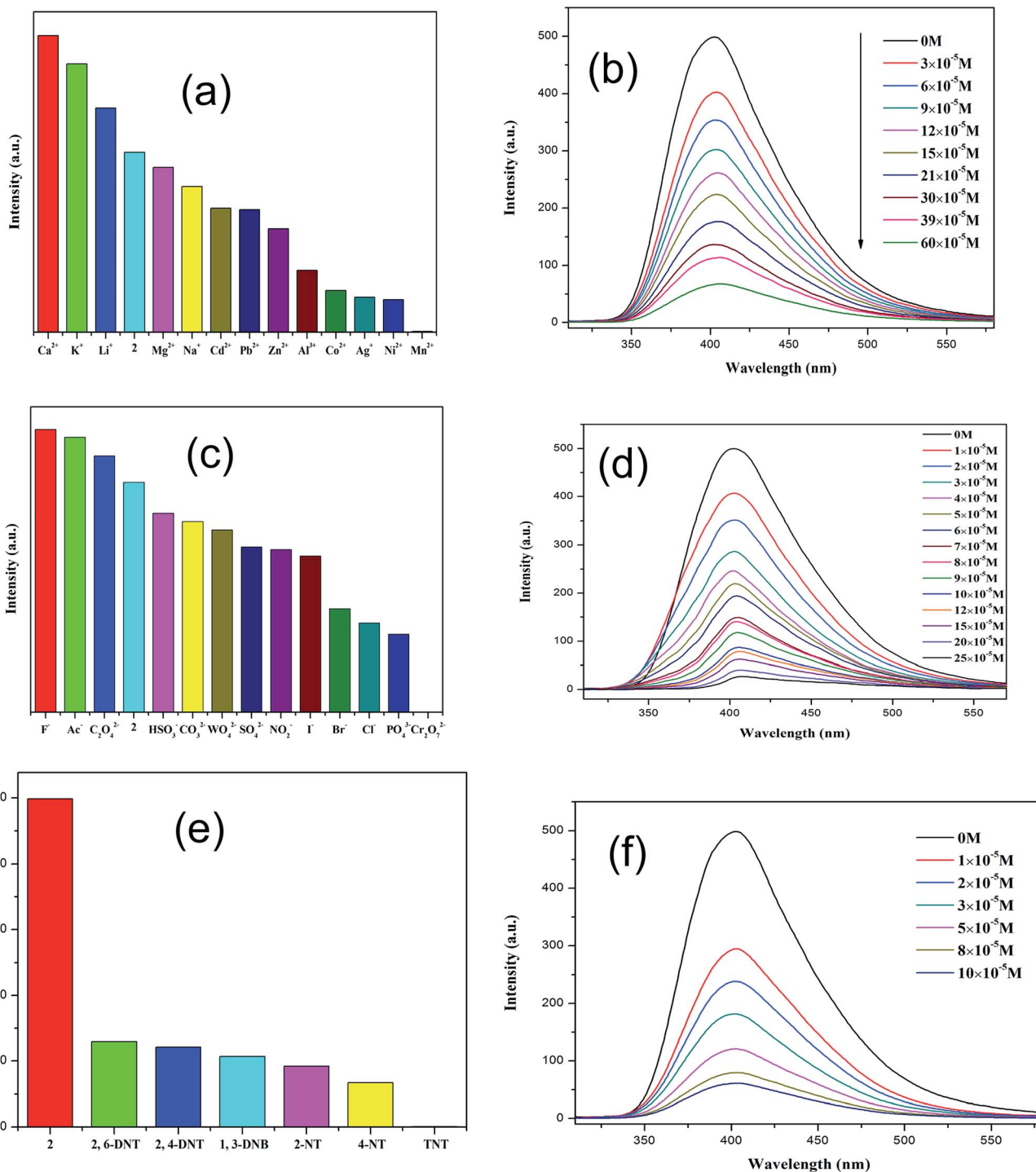
Fig. 4   (a), (c) and (e) Emission spectra of **2** in different metal ions, anions and nitro-explosives (excited at 315 nm). (b), (d) and (f) Emission spectra of **2** in different concentrations of metal ions, anions and nitro-explosives in DMF (excited at 315 nm).

shown to have a strong absorbing range from 250 to 350 nm (Fig. S9; ESI†), whereas other substances detected have no significant absorption band in this range. The strong absorption band of dbp is located at approximately 280 nm, which is largely overlapped by the absorbing band of Mn^{2+} ($Cr_2O_7^{2-}$ and series of nitro-explosives). Thus, there is competition for the absorption of the light source energy between the analytes and

dbp from 250 to 350 nm. Combined with the absorption and luminescent spectra, it was suggested that the energy absorbed by the dbp is transferred to the Mn^{2+} ($Cr_2O_7^{2-}$ and series of nitro-explosives) analytes, resulting in quenching feature in the luminescence intensity of **1–2**. The quenching mechanism obtained here was in agreement with that proposed previously by others.[28–31]
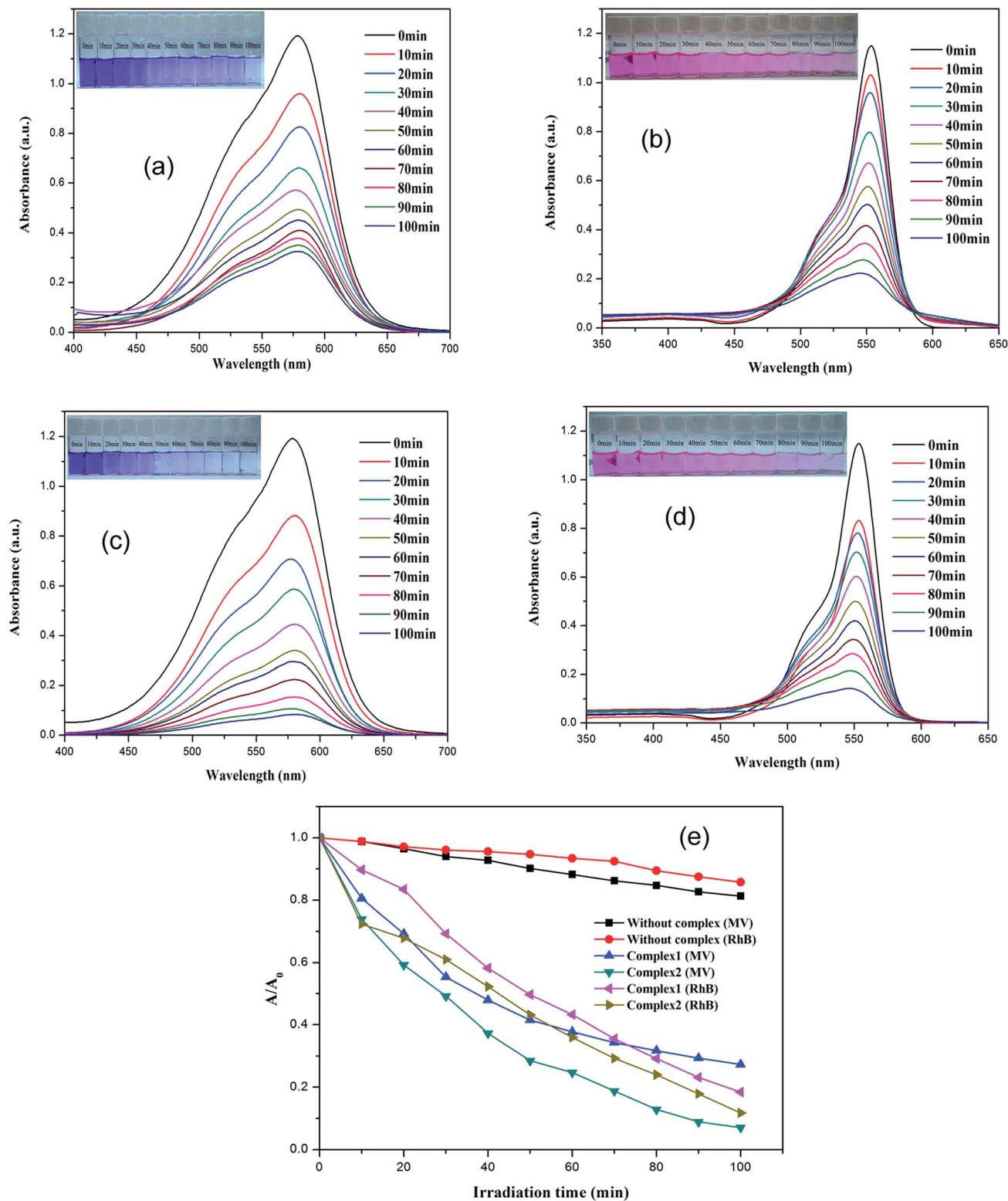
Fig. 5 (a–d) UV-Vis absorption spectra of the MV/RhB solution during the decomposition reaction under irradiation with a 500 W Hg lamp, in the presence of 1–2; (e) photodegradation of MV/RhB solution with the change in A/A_0 of 1–2, and the control experiments without any catalyst and with metal ions.

As is known, fast and easy regeneration methods are two important issues for the recyclable performance. To determine the recyclable performance of 1–2, samples of 1–2 were immersed in an DMF solution of TNT (10^{-3} M) for 5 minutes to form TNT@1 and TNT@2, and then TNT@1 and TNT@2 were washed several times with DMF. The luminescence intensity of

the recycled **1–2** were consistent with that of the original ones, although three runs were performed (Fig. S10; ESI†). The results indicate that **1–2** is still stable and that **1–2** can be recycled by a fast and simple method.

Photocatalytic activities

The dyes, MV and RhB were selected as model organic contaminants for a study of the photocatalytic activities of **1–2**. As shown in Fig. 5, the absorption peaks of MV and RhB obviously decrease with increasing of reaction time in the presence of **1–2**. The calculated results show that the degradation rate of MV is 72.7% for **1**, and 93.0% for **2**, whereas for RhB, the degradation rate for **1** and **2** is 81.6% and 88.2%, respectively. In addition, the control experiments on the degradation of organic pollutants were examined using the same reaction conditions but without the catalyst. The degradation rate of MV and RhB was 14.3% and 18.8% within 100 min under UV irradiation without a catalyst. As the previous photocatalytic results show, the photocatalytic performance of **2** is the better one because of its compacted structural features and stability. So, the final structure may influence its photocatalytic activities. In order to evaluate reproducible abilities of the as-synthesized photocatalysts, the repeated photocatalytic degradation with a constant MV/RhB concentration was determined, using complex **2** as an example. The degradation rates of **2** showed no significant reduction when the photocatalysts were used five times in the same procedures (Fig. S11a and b; ESI†), which suggested that the photocatalytic activities have good reproducibility. After photocatalysis, the PXRD patterns of **2** were similar to the simulated one, implying that **2** maintains its structural interlinkage after the photocatalysis reaction (Fig. S3; ESI†). A Cd-based MOF consisting of an amide-inserted flexible multicarboxylate ligand was reported by Wang *et al.*,[32d] however, the Cd-based MOF shows a low photocatalytic activity and only 47.9% of the RhB was degraded within 8 h. Wang *et al.* also explained that its narrow photoresponse region and low quantum yield limit its photocatalytic activity to some extent. An Anderson-type polyoxometalate-based metal–organic complex was hydrothermally synthesized at different pH ranges, and this showed that the removal of RhB dyes was almost negligible, but it showed a good photocatalysis selectivity for MV of 95.3%.[32e] The UV-Vis-near infrared spectra confirmed that **1–2** can be activated by radiation from the UV and visible light regions (Fig. S11c; ESI†). A possible photocatalytic mechanism for the previously described degradation process was proposed and is given in Scheme S2 (ESI†). When the absorbed energy is equal to or higher than its band gap energy (LUMO and the HOMO) of the materials **1–2**, the HOMO seized one electron from one water molecule and then go back to stable state. When the HOMO captured one electron from one water molecule it then goes back to the stable state. The water molecule was oxidized into a $\cdot$OH. Meanwhile, the electron of the LUMO reduced one O_2 to one O_2^- by the combination of electrons (e^-), which also changed to $\cdot$OH. Finally, the complete $\cdot$OH radical active works as an oxidizing agent to decompose MV/RhB.[32–35]

In summary, two MOFs of **1–2** were successfully synthesized, and these could be used for the quick and sensitive detection of

ions, cations and explosives using a fluorescence quenching technique. High stability and recyclability of **1–2** make them outstanding candidates for photocatalytic reactions. The present work is a promising approach for the design of MOF-based fluorescence sensors and photocatalytic reactions and this will probably be useful for more practical applications in the future.

References

1 (*a*) P. Cui, Y. Ma, H. Li, B. Zhao, J. Li, P. Cheng, P. B. Balbuena and H. C. Zhou, *J. Am. Chem. Soc.*, 2012, **134**, 18892; (*b*) H. Fu, C. Qin, Y. Lu, Z. Zhang, Y. Li, Z. Su, W. Li and E. Wang, *Angew. Chem., Int. Ed.*, 2012, **124**, 8109.

2 (*a*) L. Du, Z. Lu, K. Zheng, J. Wang, X. Zheng, Y. Pan, X. You and J. Bai, *J. Am. Chem. Soc.*, 2013, **135**, 562; (*b*) J. Q. Liu, G. L. Liu, C. Y. Gu, W. C. Liu, J. W. Xu, B. H. Li and W. J. Wang, *J. Mater. Chem. A*, 2016, **4**, 11630; (*c*) J. Q. Liu, J. Wu, F. M. Li, W. C. Liu, B. H. Li, J. Wang, Q. L. Li, R. Yadav and A. Kumar, *RSC Adv.*, 2016, **6**, 31161; (*d*) B. H. Li, J. Wu, J. Q. Liu, C. Y. Gu, J. W. Xu, M. M. Luo, R. Yadav, A. Kumar and S. R. Batten, *ChemPlusChem*, 2016, **81**, 885.

3 Y. N. Gong, Y. L. Huang, L. Jiang and T. B. Lu, *Inorg. Chem.*, 2014, **53**, 9457.

4 (*a*) Z. C. Hu, B. J. Deibert and J. Li, *Chem. Soc. Rev.*, 2014, **43**, 5815; (*b*) J. N. Hao and B. Yan, *J. Mater. Chem. A*, 2015, **3**, 4788; (*c*) X. Y. Xu, Q. C. Chen, Y. D. Yu and X. C. Huang, *Inorg. Chem.*, 2016, **55**, 75.

5 (*a*) H. C. Zhou, J. R. Long and O. M. Yaghi, *Chem. Rev.*, 2012, **112**, 673; (*b*) J. R. Long and O. M. Yaghi, *Chem. Soc. Rev.*, 2009, **38**, 1213; (*c*) H. Furukawa, K. E. Cordova, M. O'Keeffe and O. M. Yaghi, *Science*, 2013, **341**, 1230444; (*d*) S. L. Li and Q. Xu, *Energy Environ. Sci.*, 2013, **6**, 1656.

6 (*a*) C. Y. Sun, X. L. Wang, X. Zhang, C. Qin, P. Li, Z. M. Su, D. X. Zhu, G. G. Shan, K. Z. Shao, H. Wu and J. Li, *Nat. Commun.*, 2013, **4**, 2717; (*b*) J. Q. Liu, J. Wu, F. M. Li, W. C. Liu, B. H. Li, J. Wang, Q. L. Li, R. Yadav and A. Kumar, *RSC Adv.*, 2016, **6**, 31161.

7 (a) J. S. Qin, D. Y. Du, W. L. Li, J. P. Zhang, S. L. Li, Z. M. Su, X. L. Wang, Q. Xu, K. Z. Shao and Y. Q. Lan, *Chem. Sci.*, 2012, **3**, 2114; (b) Y. Q. Lan, S. L. Li, H. L. Jiang and Q. Xu, *Chem.–Eur. J.*, 2012, **18**, 8076; (c) S. L. Li, Y. Q. Lan, H. Sakurai and Q. Xu, *Chem.–Eur. J.*, 2012, **18**, 16302; (d) S. R. Zhang, D. Y. Du, K. Tan, J. S. Qin, H. Q. Dong, S. L. Li, W. W. He, Y. Q. Lan, P. Shen and Z. M. Su, *Chem.–Eur. J.*, 2013, **19**, 11279.

8 (a) S. R. Zhang, D. Y. Du, J. S. Qin, S. J. Bao, S. L. Li, W. W. He, Y. Q. Lan, P. Shen and Z. M. Su, *Chem.–Eur. J.*, 2014, **20**, 3589; (b) C. Q. Zhang, L. Sun, Y. Yan, J. Y. Li, X. W. Song, Y. L. Liu and Z. Q. Liang, *Dalton Trans.*, 2015, **44**, 230; (c) C. Q. Zhang, Y. Yan, Q. H. Pan, L. B. Sun, H. M. He, Y. L. Liu, Z. Q. Liang and J. Y. Li, *Dalton Trans.*, 2015, **44**, 13340; (d) L. B. Sun, H. Z. Xing, J. Xu, Z. Q. Liang, J. H. Yu and R. R. Xu, *Dalton Trans.*, 2013, **42**, 5508; (e) C. Q. Zhang, Y. Yan, L. B. Sun, Z. Q. Liang and J. Y. Li, *CrystEngComm*, 2016, **18**, 4102; (f) A. J. Lan, K. H. Li, H. H. Wu, D. H. Olson, T. J. Emge, W. Ki, M. C. Hong and J. Li, *Angew. Chem., Int. Ed.*, 2009, **48**, 2334.

9 (a) S. Pramanik, C. Zheng, X. Zhang, T. J. Emge and J. Li, *J. Am. Chem. Soc.*, 2011, **133**, 4153; (b) S. Pramanik, Z. Hu, X. Zhang, C. Zheng, S. Kelly and J. Li, *Chem.–Eur. J.*, 2013, **19**, 15964; (c) D. Banerjee, Z. Hu, S. Pramanik, X. Zhang, H. Wang and J. Li, *CrystEngComm*, 2013, **15**, 9745; (d) B. Gole, A. K. Bar and P. S. Mukherjee, *Chem.–Eur. J.*, 2014, **20**, 2276; (e) G. Liu, Y. Qin, L. Jing, G. Wei and H. Li, *Chem. Commun.*, 2013, **49**, 1699; (f) Y. S. Xue, Y. He, L. Zhou, F. J. Chen, Y. Xu, H. B. Du, X. Z. You and B. Chen, *J. Mater. Chem.*, 2013, **1**, 4525; (g) T. K. Kim, J. H. Lee, D. Moon and H. R. Moon, *Inorg. Chem.*, 2013, **52**, 589; (h) C. Zhu, W. Xuan and Y. Cui, *Dalton Trans.*, 2012, **41**, 3928.

10 I. H. Park, R. Medishetty, J. Y. Kim, S. S. Lee and J. J. Vittal, *Angew. Chem., Int. Ed.*, 2014, **53**, 5591.

11 B. Gole, A. K. Bar and P. S. Mukherjee, *Chem.–Eur. J.*, 2014, **20**, 13321.

12 (a) X. Li, C. F. Bi, Y. H. Fan, X. Zhang, X. M. Meng and L. S. Cui, *Inorg. Chem. Commun.*, 2014, **50**, 35; (b) G. G. Mohamed, M. M. Omar and A. A. Ibrahim, *Spectrochim. Acta, Part A*, 2010, **75**, 678.

13 Z. L. You, Y. Lu, N. Zhang and B. W. Ding, *Polyhedron*, 2011, **30**, 2186.

14 M. Kurmoo, *Chem. Soc. Rev.*, 2009, **38**, 1353.

15 (a) J. R. Li, R. J. Kuppler and H. C. Zhou, *Chem. Soc. Rev.*, 2009, **38**, 1477; (b) M. D. Allendorf, C. A. Bauer, R. K. Bhakta and R. J. T. Houk, *Chem. Soc. Rev.*, 2009, **38**, 1330; (c) Y. J. Cui, Y. F. Yue, G. D. Qian and B. L. Chen, *Chem. Rev.*, 2012, **112**, 1126.

16 H. Xiang, W. Y. Gao, D. C. Zhong, L. Jiang and T. B. Lu, *CrystEngComm*, 2011, **13**, 5825.

17 (a) D. Li, T. Wu, X. P. Zhou, R. Zhou and X. C. Huang, *Angew. Chem., Int. Ed.*, 2005, **44**, 4175; (b) H. Wu, J. Yang, Y. Y. Liu and J. F. Ma, *Cryst. Growth Des.*, 2012, **12**, 2272; (c) S. C. Chen, R. R. Qin, Z. H. Zhang, J. Qin, H. B. Gao, F. A. Sun, M. Y. He and Q. Chen, *Inorg. Chim. Acta*, 2012, **390**, 61; (d) C. J. Shen, T. L. Sheng, C. B. Tian, Q. L. Zhu and X. T. Wu, *Inorg. Chem. Commun.*, 2012, **17**, 142.

18 (a) Y. Wu, L. Lu, J. S. Feng, Y. L. Li, Y. C. Sun and A. Q. Ma, *J. Solid State Chem.*, 2017, **245**, 213; (b) K. L. Cao, Y. Xia, G. X. Wang and Y. L. Feng, *Inorg. Chem. Commun.*, 2015, **53**, 42; (c) H. Xu, H. C. Hu, C. S. Cao and B. Zhao, *Inorg. Chem.*, 2015, **54**(10), 4585.

19 G. M. Sheldrick, *SADABS, Program for Siemens Area Detector Absorption Corrections*, University of Göttingen, Germany, 1997.

20 L. Hou, L. N. Jia, W. J. Shi, Y. Y. Wang, B. Liu and Q. Z. Shi, *Dalton Trans.*, 2013, **42**, 3653.

21 A. L. Spek, *J. Appl. Crystallogr.*, 2003, **36**, 7.

22 (a) R. Singh, J. Mrozinski and P. K. Bharadwaj, *Cryst. Growth Des.*, 2014, **14**, 3623; (b) T. Wang, C. Zhang, Z. Ju and H. Zheng, *Dalton Trans.*, 2015, **44**, 6926; (c) F. L. Hu, W. Wu, P. Liang, Y. Q. Gu, L. G. Zhu, H. Wei and J. P. Lang, *Cryst. Growth Des.*, 2013, **13**, 5050.

23 (a) Q. Tang, S. X. Liu, Y. W. Liu, J. Miao, S. J. Li, L. Zhang, Z. Shi and Z. P. Zheng, *Inorg. Chem.*, 2013, **52**, 2799; (b) Y. T. Liang, G. P. Yang, B. Liu, Y. T. Yan, Z. P. Xi and Y. Y. Wang, *Dalton Trans.*, 2015, **44**, 13325.

24 X. Y. Dong, R. Wang, J. Z. Wang, S. Q. Zang and T. C. W. Mak, *J. Mater. Chem. A*, 2015, **3**, 641.

25 B. L. Chen, S. C. Xiang and G. D. Qian, *Acc. Chem. Res.*, 2010, **43**, 1115.

26 (a) S. R. Zhang, D. Y. Du, J. S. Qin, S. J. Bao, S. L. Li, W. W. He, Y. Q. Lan, P. Shen and Z. M. Su, *Chem.–Eur. J.*, 2014, **20**, 3589; (b) D. Tian, Y. Li, R. Y. Chen, Z. Chang, G. Y. Bu and X. H. Bu, *J. Mater. Chem. A*, 2014, **2**, 1465; (c) L. Y. Zhang, L. Y. Sun, X. Y. Li, Y. L. Tian and G. Z. Yuan, *Dalton Trans.*, 2015, **44**, 401–410.

27 (a) M. E. Germain and M. J. Knapp, *J. Am. Chem. Soc.*, 2008, **130**, 5422; (b) Z. J. Zhang, S. C. Xiang, X. T. Rao, Q. Zheng, F. R. Fronczek, G. D. Qian and B. L. Chen, *Chem. Commun.*, 2010, **46**, 7205; (c) D. X. Ma, B. Y. Li, X. J. Zhou, Q. Zhou, K. Liu, G. Zeng, G. H. Li, Z. Shi and S. H. Feng, *Chem. Commun.*, 2013, **49**, 8964; (d) X. H. Zhou, H. H. Li, H. P. Xiao, L. Li, Q. Zhao, T. Yang, J. L. Zuo and W. Huang, *Dalton Trans.*, 2013, **42**, 5718; (e) G. Y. Wang, L. L. Yang, Y. Li, H. Song, W. J. Ruan, Z. Chang and X. H. Bu, *Dalton Trans.*, 2013, **42**, 12865.

28 (a) J. Wang, J. Mei, W. Z. Yuan, P. Lu, A. J. Qin, J. Z. Sun, Y. G. Ma and B. Z. Tang, *J. Mater. Chem.*, 2011, **21**, 4056; (b) W. Wei, X. B. Huang, K. Y. Chen, Y. M. Tao and X. Z. Tang, *RSC Adv.*, 2012, **2**, 3765; (c) S. Ramachandra, Z. D. Popovic, K. S. Schuermann, F. Cucinotta, G. Calzaferri and L. D. Cola, *Small*, 2011, **7**, 1488.

29 (a) L. E. Kreno, K. Leong, O. K. Farha, M. Allendorf, R. P. Van Duyne and J. T. Hupp, *Chem. Rev.*, 2012, **112**, 1105; (b) Y. Cui, Y. Yue, G. Qian and B. Chen, *Chem. Rev.*, 2012, **112**, 1126.

30 Z. C. Hu, B. J. Deibert and J. Li, *Chem. Soc. Rev.*, 2014, **43**, 5815.

31 A. K. Chaudhari, S. S. Nagarkar, B. Joarder and S. K. Ghosh, *Cryst. Growth Des.*, 2013, **13**, 3716.

32 (a) S. S. Chen, J. Fan, T. Okamura, M. S. Chen, Z. Su, W. Y. Sun and N. Ueyama, *Cryst. Growth Des.*, 2010, **10**, 812; (b) H. Y. He, D. Collins, F. G. Dai, X. L. Zhao, G. Q. Zhang, H. Q. Ma and D. F. Sun, *Cryst. Growth Des.*,

2010, **10**, 895; (*c*) G. Li, Z. Lei and Q. M. Wang, *J. Am. Chem. Soc.*, 2010, **132**, 17678; (*d*) F. Q. Wang, C. F. Dong, Z. C. Wang, Y. R. Cui, C. M. Wang, Y. N. Zhao and G. D. Li, *Eur. J. Inorg. Chem.*, 2014, 6239; (*e*) X. L. Wang, J. J. Sun, H. Y. Lin, Z. H. Chang, G. C. Liu and X. Wang, *RSC Adv.*, 2016, **6**, 110583.

33 (*a*) H. Yang, X. W. He, F. Wang and J. Zhang, *J. Mater. Chem.*, 2012, **22**, 21849; (*b*) W. Q. Kan, B. Liu, J. Yang, Y. Y. Liu and J. F. Ma, *Cryst. Growth Des.*, 2012, **12**, 2288.

34 (*a*) J. L. Wang, C. Wang and W. B. Lin, *ACS Catal.*, 2012, **2**, 2630; (*b*) M. C. Das, H. Xu, Z. Y. Wang, G. Srinivas, W. Zhou, Y. F. Ke, V. N. Nesterov, G. D. Qian and B. L. Chen, *Chem. Commun.*, 2011, **47**, 11715.

35 (*a*) D. X. Li, C. Y. Ni, M. M. Chen, M. Dai, W. H. Zhang, W. Y. Yan, H. X. Qi, Z. G. Ren and J. P. Lang, *CrystEngComm*, 2014, **16**, 2158; (*b*) K. X. Wang and J. S. Chen, *Acc. Chem. Res.*, 2011, **44**, 531.